2018 26th Mediterranean Conference on Control and Automation (MED)
Zadar, Croatia, June 19-22, 2018

Time and Energy Optimal Trajectory Generation in Feed Drive Systems Using Kinematic Corner Smoothing with Interrupted Acceleration

Enock William Nshama[1] and Naoki Uchiyama[2]

Abstract— **This paper proposes a method of systematically generating corner smoothed trajectories for feed drive systems that offer the best trade-off between two contradicting objectives, namely, cycle time and energy consumption. An energy model for feed drive systems is used to define the bi-objective optimization problem. A geometry is subdivided into linear and corner segments, where the linear segments are defined by jerk limited acceleration profiles and the corner segments are defined using a kinematic corner smoothing technique with interrupted acceleration. By a normalized normal constraint method and a divide and conquer algorithm, Pareto fronts are generated and the best trade-off trajectory is obtained as the Pareto optimal point that minimizes both objectives. Simulation results for an industrial bi-axial machine are shown.**

I. INTRODUCTION

Feed drive systems are widely used in industrial applications, such as material handling and computer numerical control machine tools. With increasing demand for precision and high production rate in industrial processing, minimizing tracking and contour errors and cycle time have been major research interests. Many studies have been conducted focusing on reducing tracking errors [1], [2] and contouring control [3]–[5]. Corner smoothing algorithms have been studied for the purpose of reducing cycle time [6], [7]. However, in recent years, the growing concern on availability of reliable energy resources and reducing carbon footprint has prompted energy saving themed studies [8]–[11].

Cycle time and energy consumption are contradictory objectives that require multi-criteria optimization. Das and Dennis studied the drawbacks of the weighted sums of objectives method in producing uniformly spaced Pareto points and solving non-convex regions of a Pareto front [12]. Messac et al. proposed a method for generating a set of uniformly spaced Pareto points and a Pareto filter for retaining global Pareto points [13]. Hashem et al. proposed an algorithm for generating Pareto fronts with significant point-to-point trade-offs [14]. Studies have been made by He et al. in determining machining parameters, from Pareto fronts, for trading off energy consumption, cutting force and processing time [11]. In this paper, a method for generating corner smoothed trajectories with the best trade-off between time and energy is proposed. Jerk limited acceleration profiles (JLAP) [15] are used to generate trajectories for linear segments. For defining cornering trajectories, kinematic corner smoothing with interrupted acceleration (KCSIA) [7] is used. The normalized constraint method [13] is used to define the bi-objective optimization problem. The optimization problem is solved by sequential quadratic programming (SQP) [16]. A divide and conquer algorithm [14] is used to generate Pareto fronts, from which the best trade-off point is chosen.

This paper is organized as follows: Section II presents the derivation of an energy model from dynamics of a feed drive system. Section III describes the definition of optimization variables for generating JLAP trajectories in linear segments, followed in section IV by a description of KCSIA optimization variables and the constraints that bound the optimal solutions for traversing smoothed corners. The optimization problem is developed in section V, then the results are shown in section VI. Concluding remarks are given in section VII.

II. MATHEMATICAL ENERGY MODEL OF FEED DRIVE SYSTEMS

The dynamics of a conventional feed drive system can be described by a second order model [17]:

$$\boldsymbol{M}\ddot{\boldsymbol{x}}(t) + \boldsymbol{D}\dot{\boldsymbol{x}}(t) + \boldsymbol{F}\mathrm{sgn}(\dot{\boldsymbol{x}}(t)) = \boldsymbol{K}_{\mathrm{F}}\boldsymbol{i}(t), \qquad (1)$$

with

$$\boldsymbol{M} = \mathrm{diag}\{m_k\}, \quad \boldsymbol{D} = \mathrm{diag}\{d_k\}, \quad \boldsymbol{F} = \mathrm{diag}\{f_k\}$$
$$\boldsymbol{K}_{\mathrm{F}} = \mathrm{diag}\{k_{\mathrm{F},k}\}, \quad k = \{1, 2, ..., n\},$$

where m_k, d_k, f_k, and $k_{\mathrm{F},k}$ are the effective mass, viscous friction, Coulomb friction and force constant for the k^{th} axis, respectively. For n number of axes, $i \in \mathbb{R}^n$ and $x \in \mathbb{R}^n$ are vectors of RMS motor line currents and axis positions, respectively. Since AC servomotors are widely used in many industrial applications, it can be assumed, without any loss of generality, that the axes are also driven by this type of servomotors. By applying the methods presented in [9] and [10], the energy consumed by the feed drive system can be modeled. The motor RMS line voltage can be expressed as:

$$\boldsymbol{u}(t) = \boldsymbol{Z}\boldsymbol{i}(t) + \boldsymbol{K}_{\mathrm{E}}\dot{\boldsymbol{x}}(t), \qquad (2)$$

with

$$\boldsymbol{Z} = \mathrm{diag}\{z_k\}, \qquad \boldsymbol{K}_{\mathrm{E}} = \mathrm{diag}\{k_{\mathrm{E},k}\},$$

where z_k is the motor impedance, $k_{E,k}$ is the back EMF constant. The electrical power consumption is given by:

$$P(t) = \sqrt{3}\boldsymbol{u}(t)^T\boldsymbol{\Lambda}\boldsymbol{i}(t), \qquad (3)$$

*This work is sponsored in part by Ministry of Education, Culture, Sports, Science and Technology(MEXT)-Japan

[1]Enock William Nshama is with the Department of Mechanical Engineering, Toyohashi University of Technology, 441-8580 Toyohashi, Japan and the University of Dar es Salaam, Department of Mechanical and Industrial Engineering, Dar es Salaam, Tanzania. enocknshama@gmail.com

[2]Naoki Uchiyama is with the Department of Mechanical Engineering, Toyohashi University of Technology, 441-8580 Toyohashi, Japan. uchiyama@tut.jp

with $\mathbf{\Lambda} = \text{diag}\{\lambda_k\}$, where λ_k is the power factor of the k^{th} axis motor. The value of λ_k depends on motor loading, whereby, above a certain load threshold, it becomes nearly constant. The energy model of a feed drive system can be derived by combining (1) – (3) as follows:

$$\begin{aligned} E =& \int_0^T P(t)dt \\ =& \sqrt{3}\int_0^T \ddot{\boldsymbol{x}}(t)^T \mathbf{\Lambda} \boldsymbol{C_1} \ddot{\boldsymbol{x}}(t) + \dot{\boldsymbol{x}}(t)^T \mathbf{\Lambda} \boldsymbol{C_2} \dot{\boldsymbol{x}}(t) \\ &+ \|\mathbf{\Lambda} \boldsymbol{C_3} \dot{\boldsymbol{x}}(t)\|_1 + \text{tr}\left(\mathbf{\Lambda} \boldsymbol{C_4}\right) + \|\mathbf{\Lambda} \boldsymbol{C_5} \ddot{\boldsymbol{x}}(t)\|_1 \\ &+ \ddot{\boldsymbol{x}}(t)^T \mathbf{\Lambda} \boldsymbol{C_6} \dot{\boldsymbol{x}}(t)\ dt, \end{aligned} \tag{4}$$

with

$$\begin{aligned} &\boldsymbol{C_j} = \text{diag}\left\{c_{j,k}\right\}, \qquad j = \{1, 2, ..., 6\}, \\ &c_{1,k} = m_k^2 \frac{z_k}{k_{\text{F},k}^2}, \qquad c_{2,k} = d_k \left(\frac{z_k d_k}{k_{\text{F},k}^2} + \frac{k_{\text{E},k}}{k_{\text{F},k}}\right), \\ &c_{4,k} = f_k^2 \frac{z_k}{k_{\text{F},k}^2}, \qquad c_{3,k} = f_k \left(\frac{2 z_k d_k}{k_{\text{F},k}^2} + \frac{k_{\text{E},k}}{k_{\text{F},k}}\right), \\ &c_{5,k} = 2 f_k m_k \frac{z_k}{k_{\text{F},k}^2}, \quad c_{6,k} = m_k \left(\frac{2 z_k d_k}{k_{\text{F},k}^2} + \frac{k_{\text{E},k}}{k_{\text{F},k}}\right). \end{aligned}$$

III. JERK LIMITED ACCELERATION PROFILE

This section presents the JLAP [15], which is a trajectory profile obtained by subdividing a segment, to be traversed, into sections with finite jerks. Generally, a segment can consist of acceleration, constant velocity and deceleration sections. The time intervals for each section are determined in such a way that the acceleration, velocity and spacial constraints are met throughout the segment. Based on JLAP, a linear segment trajectory can be expressed as:

$$\begin{aligned} j_{a,k}(t) &= \begin{cases} j_{\text{max},k}, & t_0 \le t < t_{1,a}, \\ 0, & t_{1,a} \le t < t_{2,a}, \\ -j_{\text{max},k}, & t_{2,a} \le t < t_{3,a}, \end{cases} \\ j_{\text{con},k}(t) &= \quad 0, \qquad\qquad t_{3,a} \le t < t_{\text{con}}, \\ j_{d,k}(t) &= \begin{cases} -j_{\text{max},k}, & t_{\text{con}} \le t < t_{1,d}, \\ 0, & t_{1,d} \le t < t_{2,d}, \\ j_{\text{max},k}, & t_{2,d} \le t < t_l, \end{cases} \end{aligned} \tag{5}$$

where $j_{a,k}$, $j_{\text{con},k}$, and $j_{d,k}$ are the jerk profiles for the acceleration, constant velocity and deceleration sections, respectively, and $j_{\text{max},k}$ is the maximum jerk of the k^{th} axis. By integrating (5), the maximum acceleration, $a_{\text{acc},k}$, maximum deceleration, $a_{\text{dec},k}$, and maximum velocity, $v_{\text{con},k}$ and velocity at the end of the linear segment, $v_{e,l,k}$ can be obtained as follows:

$$\begin{aligned} a_{\text{acc},k} &= a_{s,l,k} + j_{\text{max},k} T_{1,a}, \\ a_{\text{dec},k} &= -j_{\text{max},k} T_{1,d}, \\ v_{\text{con},k} &= v_{s,l,k} + a_{s,l,k}\left(T_{1,a} + T_{2,a} + T_{3,a}\right) \\ &\quad + \frac{1}{2} j_{\text{max},k}\left(T_{1,a}^2 - T_{3,a}^2\right) + j_{\text{max},k} T_{1,a}\left(T_{2,a} + T_{3,a}\right), \\ v_{e,l,k} &= v_{\text{con},k} - \frac{1}{2} j_{\text{max},k}\left(T_{1,d}^2 - T_{3,d}^2\right) \\ &\quad - j_{\text{max},k} T_{1,d}\left(T_{2,d} + T_{3,d}\right), \end{aligned} \tag{6}$$

with

$$\begin{aligned} T_{1,a} &= t_{1,a} - t_0, & T_{1,d} &= t_{1,d} - t_{\text{con}}, \\ T_{2,a} &= t_{2,a} - t_{1,a}, & T_{2,d} &= t_{2,d} - t_{1,d}, \\ T_{3,a} &= t_{3,a} - t_{2,a}, & T_{3,d} &= t_l - t_{2,d}, \\ T_{\text{con}} &= t_{\text{con}} - t_{3,a}, \end{aligned}$$

where $v_{s,l,k}$ and $a_{s,l,k}$ are the velocity and acceleration at the start of the linear segment for the k_{th} axis, respectively. $T_{1,a}$, $T_{2,a}$, and $T_{3,a}$ are the time intervals for positive, zero and negative jerks in the acceleration section, respectively. T_{con} is the time interval for the constant velocity section. $T_{1,d}$, $T_{2,d}$, and $T_{3,d}$ are the time intervals for negative, zero and positive jerks in the deceleration section, respectively. For known segment length, boundary conditions of velocity and acceleration and axial limits (i.e. jerk, acceleration and velocity limits), the linear segment trajectory can be defined by the time intervals $T_{1,a}$, $T_{2,a}$, $T_{3,a}$, T_{con}, $T_{1,d}$, $T_{2,d}$ and $T_{3,d}$ with the time optimization problem described as:

$$\begin{aligned} &\min_{\boldsymbol{\mu}_l} T_l, \\ &\boldsymbol{\mu}_l = \left[T_{1,a}, T_{2,a}, T_{3,a}, T_{\text{con}}, T_{1,d}, T_{2,d}, T_{3,d}\right]^T, \end{aligned} \tag{7}$$

with

$$T_l = T_{1,a} + T_{2,a} + T_{3,a} + T_{\text{con}} + T_{1,d} + T_{2,d} + T_{3,d}.$$

IV. KINEMATIC CORNER SMOOTHING WITH INTERRUPTED ACCELERATION

The KCSIA is a 2D corner smoothing approach that generates trajectories by analytically calculating the cornering velocity, and duration while setting the tangential acceleration, at the start and end of the cornering motion, to zero [7]. Based on JLAP, it exploits the axial limits of the feed drives to plan near time optimal cornering trajectories while maintaining a user-specified cornering tolerance ε. The resulting cornering trajectory is then blended with the interconnecting linear segments by equating the accelerations and velocities at the adjoining points, hence, ensuring C^2 continuity of motion transition. Fig. 1 shows $\boldsymbol{p}_s$, $\boldsymbol{p}_m$, $\boldsymbol{p}_e$ which are the starting, middle and ending points of the corner trajectory originally located at $\boldsymbol{p}_c$.

The motion is subdivided into positive, zero and negative

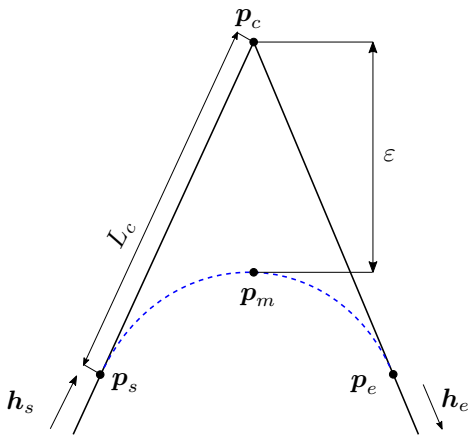

Fig. 1: Kinematic corner smoothing.

jerk sections as follows:

$$j_k(t) = \begin{cases} j_{c,k}, & t_0 \le t < t_{1,c}, \\ 0, & t_{1,c} \le t < t_{2,c}, \\ -j_{c,k}, & t_{2,c} \le t < t_c, \end{cases}$$
$$a_k(t) = \begin{cases} j_{c,k}\left(t - t_0\right), & t_0 \le t < t_{1,c}, \\ j_{c,k}\left(t_{1,c} - t_0\right), & t_{1,c} \le t < t_{2,c}, \\ j_{c,k}\left(t_{1,c} + t_{2,c} - t_0 - t\right), & t_{2,c} \le t < t_c, \end{cases} \tag{8}$$

with

$$j_{c,k} = \frac{v_{e,c,k} - v_{s,c,k}}{T_{1,c}\left(T_{1,c} + T_{2,c}\right)}, \qquad k = \{1, 2\},$$
$$T_{1,c} = t_{1,c} - t_0 = t_c - t_{2,c}, \qquad v_{s,c,k} = V_c h_{s,k}$$
$$T_{2,c} = t_{2,c} - t_{1,c}, \qquad v_{e,c,k} = V_c h_{e,k},$$

where $j_{c,k}$ is the cornering jerk, V_c is the tangential velocity magnitude at the start and end of the corner segment. $h_{s,k}$ and $h_{e,k}$ are the components of velocity unit vectors on the k^{th} axis at the start and end of the corner segment, respectively. $v_{s,c,k}$ and $v_{e,c,k}$ are the velocities at the start and end of the corner segment, respectively. $T_{1,c}$, $T_{2,c}$ are the time intervals for non-zero and zero jerk sections of the cornering trajectory, respectively. The total displacement in each axis, $\Delta s_{c,k}$ derived by successive integration of (8),

$$\Delta s_{c,k} = \left(v_{s,c,k} + \frac{1}{2} j_{c,k} T_{1,c}\left(T_{1,c} + T_{2,c}\right)\right)\left(2T_{1,c} + T_{2,c}\right), \tag{9}$$

is used for expressing the euclidean length, L_c as follows:

$$L_c = \frac{\Delta s_k}{\left(h_{s,k} + h_{e,k}\right)}. \tag{10}$$

From (10), $\boldsymbol{p}_s$, $\boldsymbol{p}_m$ and $\boldsymbol{p}_e$ can be obtained as follows:

$$\begin{aligned} \boldsymbol{p}_s &= \boldsymbol{p}_c - L_c \boldsymbol{h}_s, \\ \boldsymbol{p}_m &= \boldsymbol{p}_s + \boldsymbol{v}_{s,c}\left(T_{1,c} + \frac{1}{2}T_{2,c}\right) + \boldsymbol{j}_c\left(\frac{1}{2}T_{1,c}\left(\frac{T_{2,c}}{2}\right)^2\right) \\ &\quad + \boldsymbol{j}_c\left(\frac{1}{6}T_{1,c}^3 + \frac{1}{2}T_{1,c}^2\left(\frac{T_{2,c}}{2}\right)\right), \\ \boldsymbol{p}_e &= \boldsymbol{p}_c + L_c \boldsymbol{h}_e, \end{aligned} \tag{11}$$

whereby a cornering constraint can be expressed as:

$$\|\boldsymbol{p}_c - \boldsymbol{p}_m\|_2 - \varepsilon = 0. \tag{12}$$

For a given geometry, cornering tolerance and axial limits, (8)-(12) show that the cornering trajectory can be defined by V_c, $T_{1,c}$ and $T_{2,c}$ with the time optimization problem described as:

$$\min_{\boldsymbol{\mu}_c} T_c, \qquad \boldsymbol{\mu}_c = \left[V_c, T_{1,c}, T_{2,c}\right]^T, \tag{13}$$

with

$$T_c = 2T_{1,c} + T_{2,c}.$$

V. PARETO OPTIMAL TRAJECTORY GENERATION

This section presents a method of determining a trajectory that trades off cycle time with energy saving for a given geometry, axial limits and cornering tolerance by extending the methods in [7] and [13]. By utilizing the energy model in section II, JLAP for linear segments in section III and KCSIA in section IV, a bi-objective optimization problem is presented as follows:

$$\begin{aligned} &\min_{\boldsymbol{\mu}} \left\{T_{\text{tot}}(\boldsymbol{\mu}), E_{\text{tot}}(\boldsymbol{\mu})\right\}, \\ &\boldsymbol{\mu} = \left[\boldsymbol{\mu}_{l,1}, \boldsymbol{\mu}_{c,1}, \boldsymbol{\mu}_{l,2}, \boldsymbol{\mu}_{c,2}, \ldots, \boldsymbol{\mu}_{l,n_l}, \boldsymbol{\mu}_{c,n_c}\right]^T, \end{aligned} \tag{14}$$

subject to

$$g_r(\boldsymbol{\mu}) = 0, \qquad r = \{1, 2, \ldots, n_g\}, \tag{15}$$
$$q_y(\boldsymbol{\mu}) \le 0, \qquad y = \{1, 2, \ldots, n_q\}, \tag{16}$$
$$-\boldsymbol{\mu} \le \mathbf{0}, \tag{17}$$

with

$$\begin{aligned} T_{\text{tot}}(\boldsymbol{\mu}) &= \sum_{m=1}^{n_l} T_{l,m}(\boldsymbol{\mu}_{l,m}) + \sum_{m=1}^{n_c} T_{c,m}(\boldsymbol{\mu}_{c,m}), \\ E_{\text{tot}}(\boldsymbol{\mu}) &= \sum_{m=1}^{n_l} E_{l,m}(\boldsymbol{\mu}_{l,m}) + \sum_{m=1}^{n_c} E_{c,m}(\boldsymbol{\mu}_{c,m}), \end{aligned} \tag{18}$$

where T_{tot} is the cycle time, E_{tot} is the total energy consumption, $\boldsymbol{\mu}$ is the optimization variable vector, n_l is the number of linear segments, n_c is the number of corner segments. g_r is the r^{th} equality constraint, q_y is the y^{th} inequality constraint, n_g and n_q are the number of equality and inequality constraints, respectively. By independently

optimizing each objective in (14), the minima and maxima of the objectives can be obtained as follows:

$$\begin{aligned} T_{\min} &= T_{\text{tot}}(\boldsymbol{\mu}_T), & E_{\max} &= E_{\text{tot}}(\boldsymbol{\mu}_T), \\ T_{\max} &= T_{\text{tot}}(\boldsymbol{\mu}_E), & E_{\min} &= E_{\text{tot}}(\boldsymbol{\mu}_E), \end{aligned} \tag{19}$$

with

$$\boldsymbol{\mu}_T = \arg\min_{\boldsymbol{\mu}} T_{\text{tot}}(\boldsymbol{\mu}), \qquad \boldsymbol{\mu}_E = \arg\min_{\boldsymbol{\mu}} E_{\text{tot}}(\boldsymbol{\mu})$$

The objectives in (14) can be normalized using (19) as follows:

$$\tilde{T}_{\text{tot}}(\boldsymbol{\mu}) = \frac{T_{\text{tot}}(\boldsymbol{\mu}) - T_{\min}}{\Delta T}, \quad \tilde{E}_{\text{tot}}(\boldsymbol{\mu}) = \frac{E_{\text{tot}}(\boldsymbol{\mu}) - E_{\min}}{\Delta E}, \tag{20}$$

with

$$\Delta T = T_{\max} - T_{\min}, \qquad \Delta E = E_{\max} - E_{\min},$$

where ΔT and ΔE are the time and energy saving potentials, respectively. The coordinates $(T_{\min}, E_{\max})$ and $(T_{\max}, E_{\min})$ on a time-energy plane can be transformed into $\boldsymbol{P}_T$(0,1) and $\boldsymbol{P}_E$(1,0), respectively, on a normalized time-energy plane. By applying (20) in (14), the optimization problem can be reformulated as:

$$\min_{\boldsymbol{\mu}} \tilde{E}_{\text{tot}}(\boldsymbol{\mu}), \tag{21}$$

subject to (15)–(17) and:

$$\boldsymbol{N}^T \left[\boldsymbol{\psi} - \boldsymbol{P}\right] \leq 0, \tag{22}$$

with

$$\boldsymbol{N} = \boldsymbol{P}_E - \boldsymbol{P}_T = [1, -1]^T, \tag{23}$$

$$\boldsymbol{\psi} = \left[\tilde{T}_{\text{tot}}(\boldsymbol{\mu}), \tilde{E}_{\text{tot}}(\boldsymbol{\mu})\right]^T, \tag{24}$$

$$\boldsymbol{P} = (1-\zeta)\,\boldsymbol{P}_T + \zeta \boldsymbol{P}_E, \qquad 0 \leq \zeta \leq 1, \tag{25}$$

where ζ is a weighting factor. Based on the divide and conquer algorithm in [14] a set of relevant Pareto optimal points, $\boldsymbol{\Psi}$, can be generated by specifying a minimum significance level between successive points. The best trade-off point can be obtained as follows:

$$\boldsymbol{\psi}^* = \arg\min_{\boldsymbol{\psi}} \|\boldsymbol{\Psi}\|_2. \tag{26}$$

In trajectory generation, it is assumed that the first and last segments are linear, hence, $n_c = n_l - 1$. The constraints that apply to the m^{th} linear segment, are as follows:

$$\left.\begin{aligned} a_{\text{acc},k,m}^2 - a_{\text{lim},k}^2 &\leq 0 \\ a_{\text{dec},k,m}^2 - a_{\text{lim},k}^2 &\leq 0 \\ v_{\text{con},k,m}^2 - v_{\text{lim},k}^2 &\leq 0 \end{aligned}\right\}, \forall m, \tag{27}$$

$$\left.\begin{aligned} a_{s,l,k,m} &= 0 \\ a_{e,l,k,m} - a_{s,c,k,m} &= 0 \\ v_{s,l,k,m} &= 0 \\ v_{e,l,k,m} - v_{s,c,k,m} &= 0 \\ \Delta s_{l,k,m} + \left[L_{c,m} - L_m\right] h_{s,k,m} &= 0 \end{aligned}\right\}, m = 1, \tag{28}$$

$$\left.\begin{aligned} a_{s,l,k,m} - a_{e,c,k,m-1} &= 0 \\ a_{e,l,k,m} - a_{s,c,k,m} &= 0 \\ v_{s,l,k,m} - v_{e,c,k,m-1} &= 0 \\ v_{e,l,k,m} - v_{s,c,k,m} &= 0 \\ \Delta s_{l,k,m} + \\ \left[L_{c,m-1} + L_{c,m} - L_m\right] h_{s,k,m} &= 0 \end{aligned}\right\}, m \neq [1, n_l], \tag{29}$$

$$\left.\begin{aligned} a_{s,l,k,m} - a_{e,c,k,m-1} &= 0 \\ a_{e,l,k,m} &= 0 \\ v_{s,l,k,m} - v_{e,c,k,m-1} &= 0 \\ v_{e,l,k,m} &= 0 \\ \Delta s_{l,k,m} + \left[L_{c,m-1} - L_m\right] h_{s,k,m} &= 0 \end{aligned}\right\}, m = n_l, \tag{30}$$

$$j_{\max,k,m} - j_{\text{lim},k,m} = 0, \forall m, \tag{31}$$

where $j_{\text{lim},k,m}$, $a_{\text{lim},k}$, and $v_{\text{lim},k}$ are the jerk, acceleration and velocity limits. The indices s, e, l, and c refer to a start of a segment, an end of a segment, linear segment and corner segment, respectively. L_m is the length of the m^{th} linear segment before corner smoothing. For the m^{th} corner trajectory defined by KCSIA, the following are the optimization constraints:

$$\left.\begin{aligned} j_{c,k,m}^2 - j_{\text{lim},k,m}^2 &\leq 0 \\ \left(j_{c,k} T_{1,c}\right)^2 - a_{\text{lim},k,m}^2 &\leq 0 \\ v_{s,c,k,m}^2 - v_{\text{lim},k,m}^2 &\leq 0 \\ v_{e,c,k,m}^2 - v_{\text{lim},k,m}^2 &\leq 0 \\ \|\boldsymbol{p}_{c,m} - \boldsymbol{p}_{mid,m}\|_2 - \varepsilon_m &\leq 0 \end{aligned}\right\}, \forall m. \tag{32}$$

It can be seen that the cornering constraints in (32) are inequality constraints, which is in contrast with (12). The usage of an inequality constraint instead of an equality constraint adds a degree of freedom in solving (14). The optimization problem is solved by the sequential quadratic programming (SQP) [16] method.

VI. OPTIMIZATION RESULTS

System parameters of an industrial biaxial feed drive system (see Fig. 2), consisting of AC servomotors and a table, are used to create optimal trajectories. Table I shows the plant parameters used for trajectory optimization. The axial limits are $j_{\text{lim},k} = 200{,}000\,\text{mm/s}^3$, $a_{\text{lim},k} = 500\,\text{mm/s}^2$, $v_{\text{lim},k} = 80\,\text{mm/s}$.

The contour in Fig. 3 is used to generate Pareto optimal corner smoothed trajectories at $\varepsilon = 50\,\mu$m at each corner. The contour consists of $157.5°$, $45°$ and $90°$ corners which are representative angles for obtuse, acute and right angled corners . The zoomed portion in Fig. 3 shows smoothed trajectories generated by KCSIA in section IV.

The optimization problem in section V is solved by SQP in a MATLAB environment on a laptop computer with 2.50 GHz CPU, 8 GB RAM and Windows 10 operating system. In order to generate Pareto fronts of the optimization results, a significance level of 0.01 is used in the divide and conquer

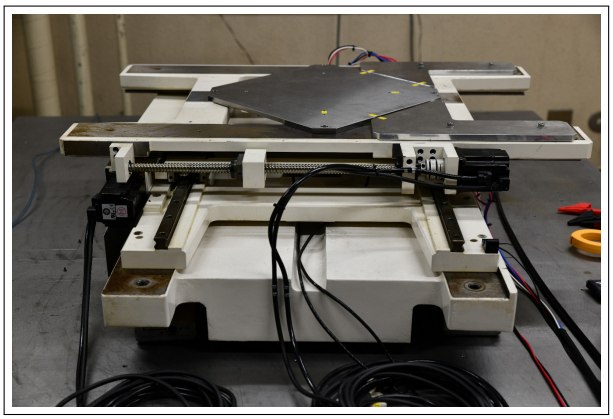

Fig. 2: Industrial biaxial feed drive system.

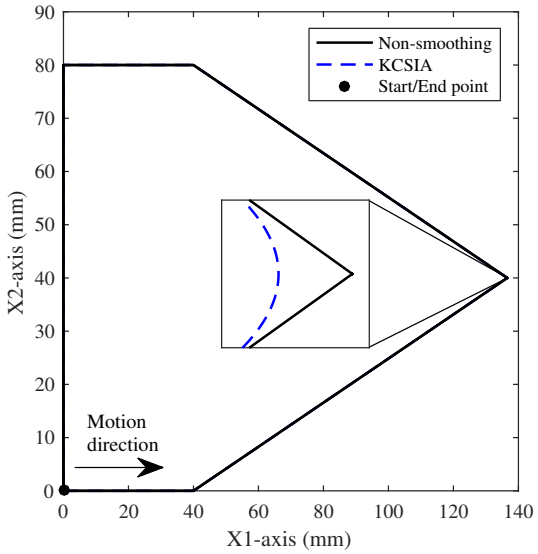

Fig. 3: The contour used for optimal trajectory generation.

algorithm.

Fig. 4 shows the trajectory optimization results for the cases of KCSIA and no smoothing (i.e. $\varepsilon = 0\,\mu$m). It can be seen that the KCSIA Pareto front is better than that for the non-smoothing case, where KCSIA produces not only the fastest cycle time, in a time optimal setting, but also the least energy in an energy optimal setting. The KCSIA trade-off point is 2.183 s faster than the energy optimal result and consumes 2.940 J less than the time optimal result. It utilizes 63.96 % and 70.33 % of the time and energy saving potentials, respectively.

Figs. 5 and 6 show the generated path acceleration and velocity profiles of the time optimal, best trade-off and energy optimal scenarios for the KCSIA and non-smoothing case. In all the optimal outcomes, KCSIA has the fastest cycle time. The path velocity profiles for the best trade-off scenarios compromises cycle time with reduced path velocities.

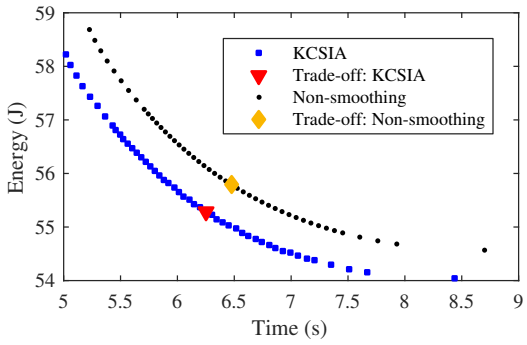

Fig. 4: The Pareto front representation of the optimization results

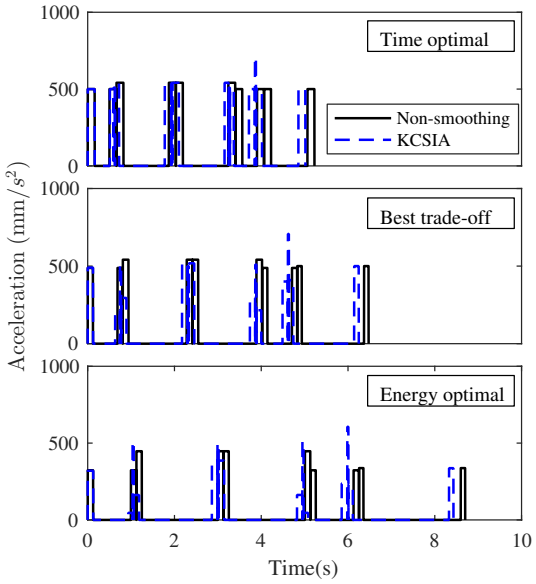

Fig. 5: The generated path velocity profile for time optimal, energy optimal and best trade off cases.

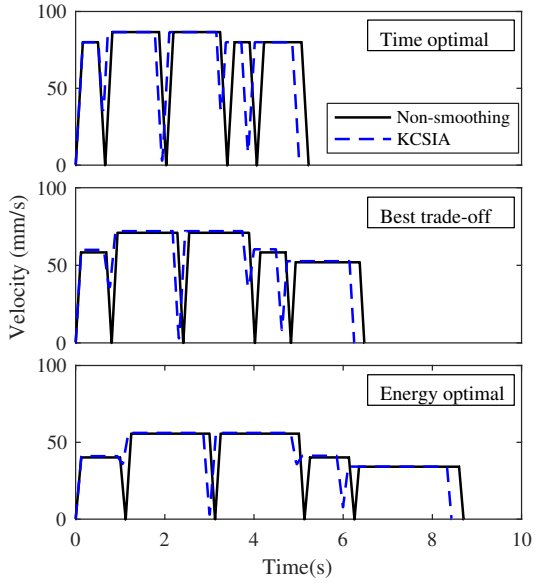

Fig. 6: The generated path acceleration profile for time optimal, energy optimal and best trade off cases.

TABLE I: Plant parameters

k^{th} axis	m_k(Ns^2/mm)	d_k(Ns/mm)	f_k(N)	$k_{\mathrm{F},k}$(N/A)	$k_{\mathrm{E},k}$(Vs/mm)	$z_k(\Omega)$	λ_k
1	0.08	0.56	48.00	124.76	0.14	10.00	0.43
2	0.09	0.80	58.00	200.22	0.20	15.00	0.45

VII. CONCLUSION

This paper presents a method for generating corner smoothed trajectories with the best trade-off between cycle time and energy for feed drive systems. The presented method considers kinematic corner smoothing techniques with interrupted acceleration and jerk limited acceleration profiles for linear segments, where a bi-objective optimization problem is solved and the best trade-off trajectory is obtained. Optimization results show that the trade-off point gives the best compromise between cycle time and energy.

Experimental verification of the optimization results is planned. Cutting forces are a major source of energy consumption during machining. As future works, a model of cutting forces will be incorporated into the existing optimization problem.

ACKNOWLEDGMENT

The authors would like to thank the Machine Tool Technologies Research Foundation, San Francisco, USA and Magnescale Co., Ltd., Kanagawa, Japan for their support.

REFERENCES

[1] M. R. Msukwa, N. Uchiyama, and B. D. Bui, "Adaptive nonlinear sliding mode control with a nonlinear sliding surface for feed drive systems," in *2017 IEEE International Conference on Industrial Technology (ICIT)*, 2017, pp. 732–737.

[2] J. Yang, D. Aslan, and Y. Altintas, "Identification of workpiece location on rotary tables to minimize tracking errors in five-axis machining," *International Journal of Machine Tools and Manufacture*, vol. 125, pp. 89 – 98, 2018.

[3] K. R. Simba, G. Heppeler, B. D. Bui, Y. M. Hendrawan, O. Sawodny, and N. Uchiyama, "Bézier curve based trajectory generation and nonlinear friction compensation for feed drive contouring control," *IFAC-PapersOnLine*, vol. 50, pp. 1944 – 1951, 2017, 20th IFAC World Congress.

[4] B. D. Bui, N. Uchiyama, and K. R. Simba, "Contouring control for three-axis machine tools based on nonlinear friction compensation for lead screws," *International Journal of Machine Tools and Manufacture*, vol. 108, pp. 95–105, Sep. 2016.

[5] B. D. Bui and N. Uchiyama, "Sliding mode contouring controller design with adaptive friction compensation for three-axis machine tools," in *2016 American Control Conference (ACC)*. Institute of Electrical and Electronics Engineers (IEEE), Jul. 2016.

[6] B. Sencer, K. Ishizaki, and E. Shamoto, "A curvature optimal sharp corner smoothing algorithm for high-speed feed motion generation of NC systems along linear tool paths," *The International Journal of Advanced Manufacturing Technology*, vol. 76, pp. 1977–1992, Oct. 2014.

[7] S. Tajima and B. Sencer, "Kinematic corner smoothing for high speed machine tools," *International Journal of Machine Tools and Manufacture*, vol. 108, pp. 27–43, Sep. 2016.

[8] N. Uchiyama, Y. Ogawa, A. E. K. Mohammad, S. Sano, and K. Yamazaki, "Energy saving control in five-axis machine tools using contouring control," in *2013 European Control Conference (ECC)*, Jul. 2013, pp. 797–802.

[9] N. Uchiyama, Y. Honda, and S. Sano, "Residual vibration suppression and energy saving in industrial machines using a trapezoidal velocity profile," in *2014 American Control Conference*. Institute of Electrical and Electronics Engineers (IEEE), Jun. 2014.

[10] N. Uchiyama, K. Goto, and S. Sano, "Analysis of energy consumption in fundamental motion of industrial machines and experimental verification," in *2015 American Control Conference (ACC)*. Institute of Electrical and Electronics Engineers (IEEE), Jul. 2015, pp. 2179–2184.

[11] K. He, R. Tang, and M. Jin, "Pareto fronts of machining parameters for trade-off among energy consumption, cutting force and processing time," *International Journal of Production Economics*, vol. 185, pp. 113 – 127, 2017.

[12] I. Das and J. E. Dennis, "A closer look at drawbacks of minimizing weighted sums of objectives for pareto set generation in multicriteria optimization problems," *Structural optimization*, vol. 14, pp. 63–69, Aug. 1997.

[13] A. Messac, A. Ismail-Yahaya, and C. A. Mattson, "The normalized normal constraint method for generating the pareto frontier," *Structural and Multidisciplinary Optimization*, vol. 25, pp. 86–98, Jul. 2003.

[14] I. Hashem, D. Telen, P. Nimmegeers, F. Logist, and J. V. Impe, "A novel algorithm for fast representation of a pareto front with adaptive resolution: Application to multi-objective optimization of a chemical reactor," *Computers & Chemical Engineering*, vol. 106, pp. 544 – 558, 2017.

[15] K. Erkorkmaz and Y. Altintas, "High speed CNC system design. part i: jerk limited trajectory generation and quintic spline interpolation," *International Journal of Machine Tools and Manufacture*, vol. 41, pp. 1323–1345, Jul. 2001.

[16] P. E. Gill and E. Wong, "Sequential quadratic programming methods," in *Mixed Integer Nonlinear Programming*, J. Lee and S. Leyffer, Eds. New York, NY: Springer New York, 2012, pp. 147–224.

[17] D. Prevost, S. Lavernhe, C. Lartigue, and D. Dumur, "Feed drive modelling for the simulation of tool path tracking in multi-axis high speed machining," *International Journal of Mechatronics and Manufacturing Systems*, vol. 4, p. 266, 2011.